begell house, inc.
Journal Production
50 Cross Highway
Redding, CT 06896
Phone: 1-203-938-1300
Fax: 1-203-938-1304
Begell House Production Contact : journals@begellhouse.com

Dear Corresponding Author,

Effective April 2011 Begell House will no longer provide corresponding authors with a print copy of the issue in which their article appears. Corresponding authors will now receive a pdf file of the final version of their article that has been accepted for publication.

Please note that the pdf file provided is for your own personal use and is not to be posted on any websites or distributed in any manner (electronic or print). Please follow all guidelines provided in the copyright agreement that was signed and included with your original manuscript files.

Any questions or concerns pertaining to this matter should be addressed to journals@begellhouse.com

Thank you for your contribution to our journal and we look forward to working with you again in the future.

.

Sincerely,

Michelle Amoroso

Michelle Amoroso
Production Department

Journal of Porous Media, 15 (6): 567–584 (2012)

NATURAL CONVECTION HEAT TRANSFER IN A HORIZONTAL CONCENTRIC ELLIPTIC ANNULUS CONTAINING SATURATED POROUS MEDIA

Ramadan Y. Sakr & Nabil S. Berbish*

Department of Mechanical Engineering, Faculty of Engineering, Benha University, 108 Shoubra Street, 11689, Cairo, Egypt

*Address all correspondence to Ramadan Y. Sakr E-mail: ramadan.sakr@feng.bu.edu.eg

Original Manuscript Submitted: 6/2/2010; Final Draft Received: 12/28/2010

Natural convection heat transfer in a horizontal elliptic annulus filled with saturated porous media is investigated experimentally and numerically. The inner horizontal elliptic tube is heated under constant heat flux conditions and is located concentrically in a larger isothermally cooled horizontal cylinder. Both ends of the water-saturated porous annulus are closed. The heated elliptic tube was made of copper material and has an axis ratio (AR = a/b) of 3.0. The porous media used in the experiments were made of sandstone and glass materials with different solid thermal conductivities and particle diameters. The elliptic tube orientation angle is varied from 0° to 90°, and the hydraulic radius ratio, HRR = R_o/R_i, is 6.85. The numerical solution scheme is based on a two-dimensional model, which is governed by Darcy-Boussinseq equations. The inner elliptic cylinder is heated isothermally, while the outer circular cylinder is also cooled isothermally. Discretization of the governing equations is achieved using a finite element scheme based on Galerkin method of weighted residuals. The effect of pertinent parameters such as modified Rayleigh number, Ra (Rayleigh-Darcy), orientation angle of the elliptic cylinder, δ, and the axis ratio of the elliptic cylinder, AR, is investigated. The numerical results obtained from the present model are compared with the available published results and with the present experimental results, and good agreement is found. The variation of the average Nusselt number with the investigated parameters is presented. It is concluded that the effect of modified Rayleigh number, which includes the effect of fluid properties, porous medium properties, and operating conditions on the average Nusselt number, is more significant than the effect of the geometric parameters such as the elliptic cylinder orientation angle and the elliptic cylinder axis ratio. The results showed that the average Nusselt number increases with the increase of the modified Rayleigh number. Also, the flow and heat transfer characteristics are illustrated via stream function and isotherms contours. Moreover, an empirical correlation for the average Nusselt number is obtained as a function of Rayleigh number, elliptic cylinder orientation angle, and elliptic cylinder axis ratio.

KEY WORDS: *natural convection, heat transfer, horizontal elliptic annulus, saturated porous media*

1. INTRODUCTION

Natural convection heat transfer in a horizontal porous annulus has been the subject of many investigations in recent years. The motivation of these studies was derived from their technological applications such as thermal insulation, thermal storage systems, cryogenics, nuclear reactors, and underground electrical transmission lines (Charrier-Mojtabi, 1997; Khanafer et al., 2008).

The analysis of natural convection in a cylindrical porous annulus has been studied experimentally and numerically by several investigators. The first experimental and numerical work on porous annuli was done by Caltagirone (1976), who studied a concentric cylindrical porous layer with a radius ratio of 2. For Rayleigh numbers below 65, Caltagirone observed a steady two-dimensional flow regime with two symmetric convective cells. For high Rayleigh numbers, fluctuating three-

NOMENCLATURE

A	dimensionless element area
AR	Axis ratio of the elliptic cylinder (a/b)
a	major axis length of the elliptic cylinder (m)
a_m, b_m, c_m	coefficients of Eq. (19)
b	minor axis length of the elliptic cylinder (m)
c_p	specific heat at constant pressure (J/kg K)
D	hydraulic diameter of the elliptic cylinder (m)
Da	Darcy number, Da $= K/R_i^2$
E	total number of elements
e	element
$\{F_1\}$, $\{F_2\}$	force vector, Eqs. (21a,b)
g	gravity acceleration (m/s^2)
h_x	local heat transfer coefficient (W/ m^2 K)
HRR	hydraulic radius ratio, R_o/R_i
K	permeability (m^2)
$[K_1]$, $[K_2]$	stiffness matrices, Eqs. (21a,b)
k	thermal conductivity (W/m K)
m	nodal point of the linear triangular element 1, 2, 3
N	interpolation function
$\mathrm{Nu}_{\mathrm{local}}$	local Nusselt number
Nu	average Nusselt number, defined in Eq. (17)
n	normal direction to the surface
P	circumference of the elliptic cylinder (m)
p	pressure (Pa)
q_H	heat flux (W/m^2)
R	hydraulic radius (m)
Ra*	Rayleigh number, Ra$^* = g\rho_f c_f \beta_f (T_i - T_o) R_i^3 / k_e \nu_f$
Ra	modified Rayleigh number, Ra $= g\rho_f c_f \beta_f K(T_i - T_o) R_i / k_e \nu_f$
T	temperature (°C, K)
u	x-direction velocity component (m/s)
v	y-direction velocity component (m/s)
x, y	Cartesian coordinates (m)
X, Y	dimensionless Cartesian coordinates

Greek Symbols

α	thermal diffusivity (m^2/s)
β	coefficient of thermal expansion (K^{-1})
γ	angle
Γ	domain boundary
δ	orientation angle
ν	kinematic viscosity (m^2/s)
μ	dynamic viscosity (kg/m s)
ψ	stream function (m^2/s)
Ψ	dimensionless stream function
Ω	bounded domain
θ	dimensionless temperature
ρ	density (kg/ m^3)

Subscripts

c	cold
e	effective
f	fluid
h	heater
i	inner
o	outer
r	reference

Superscripts

e	element level

dimensional effects were observed in the upper part of the layer, although the lower zone remained two-dimensional. Burns and Tien (1979) analyzed natural convection in concentric spheres and horizontal cylinders filled with a porous medium using a finite difference method. Vasseur et al. (1984) investigated a numerical study of two-dimensional laminar natural convection between horizontal concentric cylinders filled by a porous layer with internal heat generation using Darcy-Oberbeck-Boussinesq equations. Kaviany (1986) conducted the non-Darcian effects on natural convection in confined porous media between horizontal cylinders. It was reported that the effects of inertia, velocity-square, and solid boundary terms reduced the total heat transfer rate, with the boundary term being the most significant factor. Rao et al. (1987, 1988) solved the Boussinesq equations in two and three dimensions using the Galerkin finite element method. Three possible numerical solutions depending on the initial conditions were obtained for a radius ratio of 2 and Rayleigh number above 65. Numerical study of two-dimensional convection in a horizontal annulus filled with porous material in the

presence of a permeable boundary was treated by Stewart and Burns (1992). They illustrated that multicellular flows occurred at the highest Rayleigh numbers investigated. Mota and Saatdjian (1994, 1995) studied numerically natural convection in a horizontal cylindrical annulus filled with a porous medium by solving the two-dimensional Boussinesq equations using a finite difference method. A closed hysteresis loop was observed for radius ratios above 1.7 and for Rayleigh numbers above a critical value. Charrier-Mojtabi (1997) carried out a numerical investigation of two- and three- dimensional free convection flows in a saturated porous horizontal annulus. The study considered an annulus that is heated at the surface of the inner cylinder, using a Fourier-Galerkin approximation for the periodic azimuthal and axial directions, whereas a collocation–Chebyshev approximation was used in the confined radial direction. In this study, the Darcy-Boussinesq formulation was employed in terms of pressure and temperature. Saravanan and Kandaswamy (2003) conducted a linear stability analysis for a viscous flow induced by internal heat sources in a vertical annular porous region bounded by two concentric cylinders. The perturbation equations are solved by a Chebyshev collocation spectral method. The effects of the porous parameter and the radius ratio are examined. Aldoss et al. (2004) have studied the steady natural convection from a horizontal annulus filled partially or totally with a saturated porous medium where the effects of different physical parameters have been examined. It was found that an annulus completely filled with porous media has the best insulating effectiveness, and it is superior over the partially filled cases. In the case of an annulus partially filled with porous media, having the porous media located adjacent to the outer cylinder is proved to be much more effective than the inner layer case. Jha (2005) studied numerically free convection through a vertical porous annulus with mixed boundary conditions. It was concluded that the Darcy number and the radius ratio are the governing factors for heat transfer through an annular porous medium. Cheng (2006) examined the effects of the modified Darcy number, the buoyancy ratio, and the inner radius gap ratio on the fully developed natural convection heat and mass transfer in a vertical annular non-Darcy porous medium with asymmetric wall temperatures and concentrations. It was found that an increase in the buoyancy ratio or in the radius ratio led to an increase in the volume flow rate and the total heat rate added to the fluid. Leong and Lai (2006) obtained analytical solutions for natural convection in concentric cylinders with a porous sleeve using the perturbation method and Fourier transform approach. The porous sleeve was press-fitted to the inner surface of the outer cylinder. It was found that at a higher Rayleigh number, when heat convection becomes more important, it is expected that the porous sleeve thickness will play a much more important role in heat transfer. Khanafer et al. (2008) studied a numerical investigation of natural convection heat transfer within a two-dimensional, horizontal annulus that is partially filled with a fluid-saturated porous medium. Both cylinders are maintained at constant temperatures, with the inner cylinder being subjected to a relatively higher temperature than the outer one. It was illustrated that the maximum predictions of the average Nusselt number are found to depend mostly on the thermal conductivity ratio for a relatively thick porous sleeve as they exhibit better heat transfer rate when considering large thermal conductivity ratios. Kumari and Nath (2008) studied unsteady natural convection flow from a horizontal cylindrical annulus filled with a non-Darcy porous medium. It was observed that the annulus completely filled with a porous medium has the best insulating effectiveness. Aldoss (2009) investigated numerically natural convection from a horizontal annulus filled with porous medium of variable permeability using a finite volume method. The investigated annulus radius ratio was 2.0. The effect of the permeability variation on the flow and heat transfer of the annulus was presented in terms of velocity and temperature profiles, Nusselt number, skin friction coefficient, and pressure coefficient at both the inner and outer walls of the annulus. The transient natural convection flow on a heated cylinder buried in a semi-infinite liquid-saturated porous medium was studied numerically by Kumari and Nath (2009). The coupled partial differential equations governing the flow and heat transfer are cast into streamfunction–temperature formulations, and the solutions are obtained from the initial time to the time when steady state is reached. The heat transfer was found to change significantly with increasing time in small time intervals immediately after the start of the impulse change, and steady state is reached after some time.

Our survey of relevant literature saw fewer publications on natural convection in an elliptical annulus. Lee and Lee (1981) attempted to formulate the free convection problem in terms of elliptical coordinates for the symmetrical cases of oblate and prolate elliptical annuli and have performed experiments for this geometry. Elshamy et al. (1990) conducted numerically laminar natural convection between confocal horizontal elliptical cylinders and developed correlations for the average Nusselt number. Cheng and Chao (1996) employed the body-fitted curvilinear coordinate transformation method to gener-

ate a nonstaggered curvilinear coordinate system and performed a numerical study for some horizontal eccentric elliptical annuli. Saatdjian et al. (1999) studied numerically natural convection heat transfer in the annular region between porous confocal ellipses using a finite difference method. Mota et al. (2000) conducted numerically natural convection heat transfer in horizontal eccentric elliptic annuli containing saturated porous media using high-order compact finite differences on a very fine grid. It was demonstrated that the savings in heat transfer can be further improved if the elliptic annular shape is made eccentric. Chmaissem el al. (2002) carried out a numerical study of the Boussinesq model of natural convection in an annular space, having a horizontal axis bounded by circular and elliptical isothermal cylinders. The matrix system is solved using a finite element method that utilizes Cartesian coordinates and a vorticity–streamfunction formulation associated with an iterative technique. Djezzar and Daguenet (2006) studied numerically natural steady convection in space annulus between two elliptic confocal cylinders using a finite volume method. The effect of Rayleigh number and the system slope angle is investigated for Pr = 0.7. Sakr et al. (2008) investigated experimentally and numerically natural convection heat transfer in horizontal elliptic annuli. It was found that the average Nusselt number is increased with increasing Rayleigh number.

The objective of the present work is to study experimentally and numerically natural convection heat transfer in a horizontal elliptic annulus containing saturated porous media. The effect of Rayleigh number, elliptic cylinder orientation angle, and axis ratio of the elliptic cylinder on the flow and heat transfer characteristics will be presented.

2. EXPERIMENTAL SET UP

The present experimental setup, which is used to investigate natural convection heat transfer in a horizontal elliptic annulus filled with saturated porous media, is shown schematically in Fig. 1. It consists mainly of three main parts: The heating system, the cooling system, and the measuring system. The test section is designed to have the facility of changing the porous medium with different particle diameters and materials. Two concentric horizontal cylinders, the outer one circular and the inner one elliptic, are used to form an annular region. The outer cooled circular cylinder was made from copper of 200 mm outer diameter, 2 mm thickness, and 300 mm length. The inner heated elliptic cylinder was also made of copper material with a major diameter, a, of 42 mm, 2 mm thickness, and length of 300 mm. The elliptic cylinder has an axis ratio, AR (a/b), of 3.0, and the hydraulic radius ratio, HRR (R_o/R_i), is 6.85. A special mechanism is used to maintain

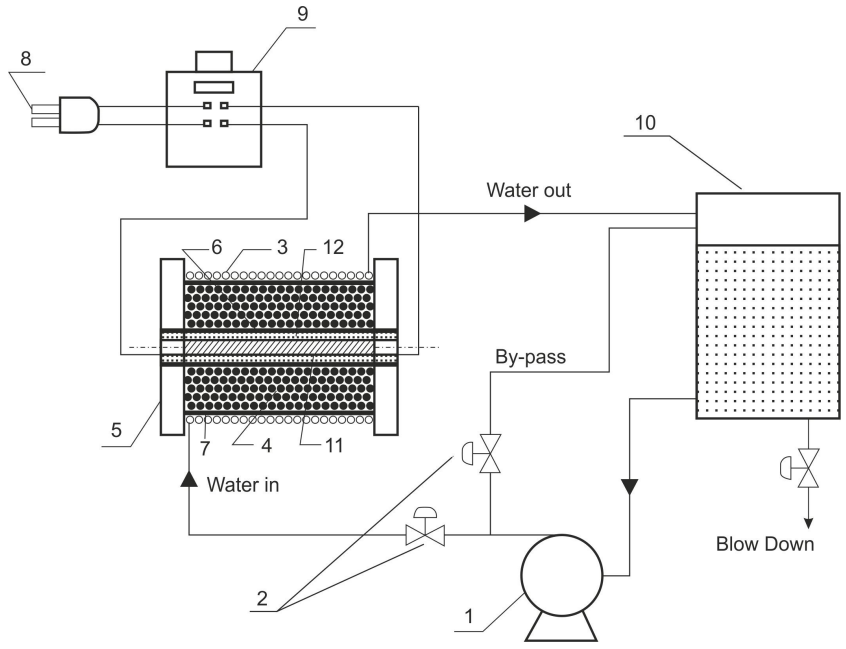

FIG. 1: Experimental setup layout

a certain angle of orientation for an inner elliptic cylinder that varies from 0° (major axis is horizontal) to 90° (major axis is vertical). The inner elliptic cylinder is heated at constant heat flux by an electric heating element. A nickel-chrome tape of 0.2 mm thickness and 4 mm width and a resistance 12 Ω is wound helically around a mica strip of 25 mm width and 2 mm thickness with a pitch of 1 mm inserted inside the elliptic cylinder; this provided the condition of approximately constant heat flux. Sixteen precalibrated copper-constantan thermocouples (0.4 mm wire diameter) were distributed circumferentially and embedded at a depth of 0.8 mm from the outer surface of the copper elliptic cylinder at mid-span distance to measure the surface temperature of the inner elliptic cylinder. The inner surface of the outer cooling cylinder is kept at a constant surface temperature (low temperature) by using a circulating water system, which is pumped through a wounded coil (with a pitch 0.5 mm) on the outer cylinder surface by a pump of 0.5 hp from a reservoir, as shown in Fig. 1. Two acrylic polystyrene covers of 300 mm diameter and 10 mm thickness are fixed to the outer cylinders and holed to permit the fixation of the inner elliptic cylinder. The space between the inner and the outer cylinders is filled with water-saturated porous media. The materials used as porous media are sandstone grains and glass beads of 6 mm diameter. Also, the effect of particles size is investigated through the test of sandstone grains of 2.7, 4.2, and 5.6 mm average diameter. In fact, the sandstone grains are not exactly spherical but have a narrow size distribution for which the equivalent diameter is determined from the lower and upper limits on the DIN standard sieving analysis. The cooling system consists of a copper coil of diameter 12.5 mm and 15 m length. Four thermocouples are distributed in the wall of the outer cylinder surface. Eighteen thermocouples are used to measure the temperature distributions through the porous annulus between the two cylinders by inserting fixed thermocouple probes from eight plugs located at mid-span distance. Another three thermocouples are used to measure the temperature of inlet and outlet cooling water and the ambient air temperature. The readings of the thermocouples are taken by using a digital thermometer with an accuracy of 0.1°C. The steady state condition is achieved after ∼3–4 hours. To confirm a uniform temperature distribution, three thermocouples are installed at the two ends and at mid-span of the tested cylinder to measure the axial temperature. The input electric power to the inner cylinder is controlled by means of a voltage regulator. Four different values of modified Rayleigh numbers (Rayleigh–Darcy) based on the equivalent hydraulic radius of the inner cylinder were utilized in the experiments, ranging from 50 to 200.

The local heat transfer coefficient, h_x, and the local Nusselt number, $\mathrm{Nu}_{\mathrm{local}}$, are calculated as follows:

$$h_x = \frac{q_H}{(T_x - T_c)} \tag{1}$$

$$\mathrm{Nu}_{\mathrm{local}} = (h_x R_i / k_e) \tag{2}$$

where q_H, T_x, T_c, R_i, and k_e are the net heat flux, local surface temperature, cold wall temperature, hydraulic radius of the inner elliptic cylinder, and effective thermal conductivity of the porous material, respectively.

The circumference of the inner elliptic cylinder is calculated from

$$P = \left[2(\pi - (\pi - 2)e^3)\right](a/2) \tag{3}$$

where; is eccentricity, which is given by

$$e = \sqrt{1 - \left(\frac{b}{a}\right)^2} \tag{4}$$

Then, the hydraulic diameter and radius of the inner cylinder are calculated, respectively, from

$$D_i = P/\pi, \quad R_i = P/2\pi \tag{5}$$

Error analysis including the temperature measurements and fluid properties shows that the average Nusselt number has uncertainty of 4.7% and the Rayleigh number is uncertain by up to 6% of the reported values.

3. PROBLEM FORMULATION AND BASIC EQUATIONS

The model considered here is a porous layer bounded between two horizontal concentric cylinders of radii R_i and R_o, as shown in Fig. 2(a). The surfaces of the two cylinders are assumed to be maintained at constant temperatures T_i and T_o, respectively, with $T_i > T_o$.

3.1 Governing Equations

The governing equations are based on steady natural convection with Boussinesq flow, Darcy flow, and negligible inertia approximation, as follows:

$$\frac{\partial u}{\partial x} + \frac{\partial v}{\partial y} = 0 \tag{6}$$

$$\frac{\partial p}{\partial x} + \frac{\mu_f}{K} u = 0 \tag{7a}$$

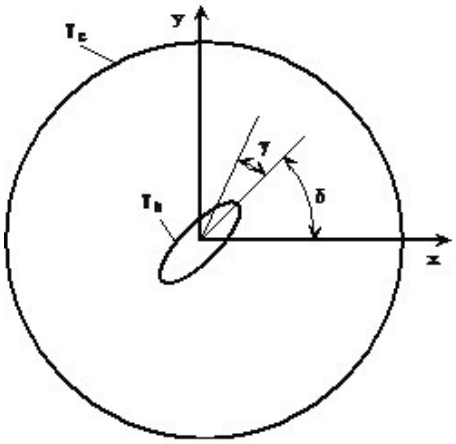

(a)

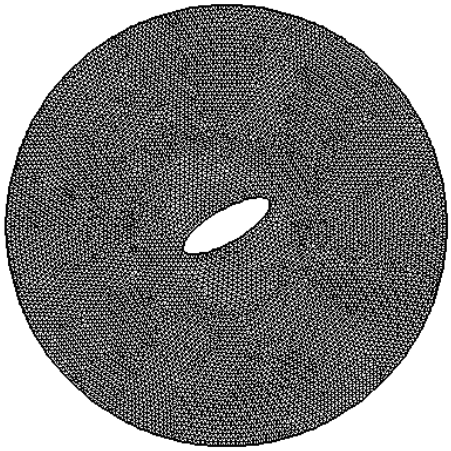

(b)

FIG. 2: Physical domain and computational grid

$$\frac{\partial p}{\partial y} + \frac{\mu_f}{K} v - \rho_f g = 0 \tag{7b}$$

$$u\frac{\partial T}{\partial x} + v\frac{\partial T}{\partial y} = \frac{k_e}{\rho_f c_f}\left(\frac{\partial^2 T}{\partial x^2} + \frac{\partial^2 T}{\partial y^2}\right) \tag{8}$$

$$\rho_f = \rho_r \left[1 - \beta_f (T - T_r)\right] \tag{9}$$

Taking the curl of Eq. (7) and using the approximation of Eq. (9), the following equations are obtained:

$$\nabla^2 \psi = -\frac{K}{\mu_f} g \rho_r \beta_f \frac{\partial T}{\partial x} \tag{10}$$

$$\nabla^2 T - \frac{\rho_f c_f}{k_e}\left[\frac{\partial \psi}{\partial y}\frac{\partial T}{\partial x} - \frac{\partial \psi}{\partial x}\frac{\partial T}{\partial y}\right] = 0 \tag{11}$$

where

$$u = \frac{\partial \psi}{\partial y}, \quad v = -\frac{\partial \psi}{\partial x} \tag{12}$$

Introducing the following nondimensional variables,

$$\theta = \frac{T - T_o}{T_i - T_o}, \quad X = \frac{x}{R_i}, \quad Y = \frac{y}{R_i}$$
$$\Psi = \frac{\psi}{\alpha}; \quad \text{where} \quad \alpha = \frac{k_e}{\rho_f c_f}$$

the governing equations reduce to

$$\nabla^2 \theta - \left(\frac{\partial \Psi}{\partial Y}\frac{\partial \theta}{\partial X} - \frac{\partial \Psi}{\partial X}\frac{\partial \theta}{\partial Y}\right) = 0 \tag{13}$$

$$\nabla^2 \Psi = \mathrm{Ra}\frac{\partial \theta}{\partial X} \tag{14}$$

where Ra = Ra*.Da.

Ra is the modified Rayleigh number and is given by Ra $= g\rho_f c_f \beta_f K(T_i - T_o)R_i/k_e \nu_f$. Ra* is Rayleigh number and is given by

$$\mathrm{Ra}^* = g\rho_f c_f \beta_f (T_i - T_o) R_i^3 / k_e \nu_f$$

Da is Darcy number and given by

$$\mathrm{Da} = K/R_i^2$$

3.2 Boundary Conditions

The boundary conditions are handled as follows:

At the inner cylinder surface:

$$\Psi = 0, \quad \theta = 1.0 \tag{15a}$$

At the outer cylinder surface:

$$\Psi = 0, \quad \theta = 0 \tag{15b}$$

3.3 Heat Transfer Calculations

The local Nusselt number at the inner cylinder surface can be calculated from the following equation:

$$\mathrm{Nu}_{\mathrm{local}} = -\left(\frac{\partial \theta}{\partial n}\right) \tag{16}$$

where n represents the direction normal to the cylinder surface. The steady state average Nusselt number at the inner cylinder surface is given by

$$\mathrm{Nu} = \frac{1}{2\pi}\int_0^{2\pi} \mathrm{Nu}_{\mathrm{local}}(\gamma)\,d\gamma \tag{17}$$

4. NUMERICAL APPROACH AND PROCEDURES

The solutions of Eqs. (13) and (14) with the boundary conditions specified by Eq. (15) are obtained numerically by using the Galerkin-based finite element method (Rao, 1982; Pepper and Heinrich, 1992). The finite element technique is used to reduce the system of governing equations into a discretized set of algebraic equations. The procedure begins with the division of the continuum region of interest into a number of simply shaped regions called elements. The grid system used in the present calculation is illustrated in Fig. 2(b). The element type used here is a linear triangular element. The approximate expressions of temperature and streamfunction in an element are given by polynomials in terms of the nodal values and interpolation functions. The interpolation functions are derived from the assumption of linear variation of temperature and streamfunction through the element and are given by the following equation:

$$\theta^e = \sum_{m=1}^{3} N_m \theta_m \tag{18a}$$

$$\psi^e = \sum_{m=1}^{3} N_m \Psi_m \tag{18b}$$

where N_m is the usual interpolation function and is defined by

$$\mathrm{Nm} = \frac{1}{2A}(am + bm\,X + cm\,Y) \tag{19}$$

where A is the element area and

$$a_1 = X_2Y_3 - X_3Y_2, \quad b_1 = Y_2 - Y_3, \quad c_1 = X_3 - X_2 \tag{20}$$

The other components are given by cyclic permutation of the subscripts in the order 1, 2, and 3. If the approximations given by Eq. (18) are substituted in the governing Eqs. (13)–(14), and the global errors are minimized using the preceding interpolation functions N_i as weighting functions, after performing the weighted integration over the domain G and the application of Green's theorem, the present model is converted into

$$[K_1]\{\theta\} = \{F_1\} \tag{21a}$$

$$[K_2]\{\Psi\} = \{F_2\} \tag{21b}$$

where

$$[K_1] = \sum_{e=1}^{E} \int_{\Omega^e} \left(\frac{\partial [N]^T}{\partial X}\cdot\frac{\partial [N]}{\partial X} + \frac{\partial [N]^T}{\partial Y}\cdot\frac{\partial [N]}{\partial Y}\right) d\Omega^e + \sum_{e=1}^{E} \int_{\Omega^e} \left(\Psi_Y [N]^T \cdot \frac{\partial [N]}{\partial X} - \Psi_X [N]^T \cdot \frac{\partial [N]}{\partial Y}\right) d\Omega^e$$

$$\{F_1\} = \sum_{e=1}^{E} \int_{\Gamma^e} \left([N]^T \frac{\partial N}{\partial X} + [N]^T \frac{\partial N}{\partial Y}\right) d\Gamma^e$$

$$[K_2] = \sum_{e=1}^{E} \int_{\Omega^e} \left(\frac{\partial [N]^T}{\partial X}\cdot\frac{\partial [N]}{\partial X} + \frac{\partial [N]^T}{\partial Y}\cdot\frac{\partial [N]}{\partial Y}\right) d\Omega^e$$

$$\{F_2\} = \sum_{e=1}^{E} \int_{\Gamma^e} [N]^T \frac{\partial [N]}{\partial X} d\Gamma^e + \int_{\Gamma^e} [N]^T \frac{\partial [N]}{\partial Y} d\Gamma^e + \sum_{e=1}^{E} \int_{\Omega^e} \mathrm{Ra}\theta [N]^T \frac{\partial [N]}{\partial X} d\Omega^e$$

and E is the total number of elements, Ω the bounded domain, Γ the domain boundary, and

$$\Psi_Y = \frac{\partial \Psi}{\partial Y}, \quad \Psi_X = \frac{\partial \Psi}{\partial X}$$

Equations (13) and (14) result in two systems of linear equations. Equations (21a) and (21b) are solved iteratively by Gauss elimination method through a FORTRAN computer code. The iterative procedure is terminated when the following relative convergence criterion is satisfied: $\left|(\Psi^{i+1} - \Psi^i)/\Psi^{i+1}\right| \le 10^{-4}$, where i denotes the iteration number performed.

5. MODEL VALIDATION

First the present numerical method is validated by solving the traditional convection problem for two concentric horizontal cylinders. The obtained results are compared with the available published data. Table 1 shows the average Nusselt number for previous researchers. In comparison with the present results, good agreement is found.

6. RESULTS AND DISCUSSION

6.1 Experimental Results

Experiments are carried out to investigate the effect of the governing parameters on the natural convection heat transfer in a horizontal elliptic annulus containing water-saturated porous media. Really, most of the governing parameters of the phenomenon are collected in a single dimensionless parameter, which is called the Rayleigh-Darcy number or modified Rayleigh, Ra, and, for simplicity, Rayleigh, which is calculated based on the temperature difference between the heated and cooled cylinders. Actually, the inner elliptic cylinder is heated under uniform heat flux conditions so the average wall temperature

TABLE 1: Comparison of the average Nusselt number for natural convection flow in a porous medium between two concentric cylinders with radius ratio of 2

Caltagirone (1976)	Rao et al. (1987)	Facas and Farouk (1983)	Bau (1984)	Facas (1995)	Present predictions	
49 × 49	10 × 10	25 × 25	30 × 44	50 × 50	10 × 18	Grid size
1.328	1.341	1.362	1.335	1.342	1.317	Ra = 50
1.829	1.861	1.902	1.844	1.835	1.865	Ra = 100

of the inner elliptic heated cylinder is utilized to obtain the values of the modified Rayleigh numbers. Also, Rayleigh number includes the effect of the fluid and the solid particle properties as well as the particle size and porosity of the porous media.

Figure 3 depicts the variation of the average Nusselt number with the orientation angle for different Rayleigh numbers. This figure shows that insignificant changes in the average Nusselt number are noticed for $\delta \leq 30^\circ$. Beyond this value, as the orientation angle increases, the average Nusselt number increases. It is found also that with the increase of Rayleigh number, the average Nusselt number increases, but with a decreasing rate. This behavior agrees well with the previous published results as in natural convection phenomenon. Nusselt number varies with Rayleigh number raised to an index power less than unity and near to a quarter. Moreover, the average Nusselt number is correlated utilizing the present experimental data plotted in Fig. 3 as a function of Rayleigh number and the orientation angle, as follows:

$$\mathrm{Nu} = 0.4624\mathrm{Ra}^{0.3117}(1+\sin\delta)^{0.2295} \qquad (22)$$

This correlation [Eq. (22)] is valid within the ranges of Rayleigh number ($50 \leq \mathrm{Ra} \leq 200$) and orientation angle ($0^\circ \leq \delta \leq 90^\circ$) with maximum relative error of $\pm 10\%$.

6.2 Numerical Simulations

Several numerical runs are carried out to investigate the effect of the modified Rayleigh number (Rayleigh-Darcy) in the range from 50 to 200, the orientation angle in the range from 0° to 90°, and the axis ratio ranged from 1.5 to 5. Figure 4 shows the variation of the average Nusselt number at the surface of the inner elliptic heated cylinder with the orientation angle. The axis ratio of the elliptic cylinder is 1.5 and $50 \leq \mathrm{Ra} \leq 200$. It is shown from this

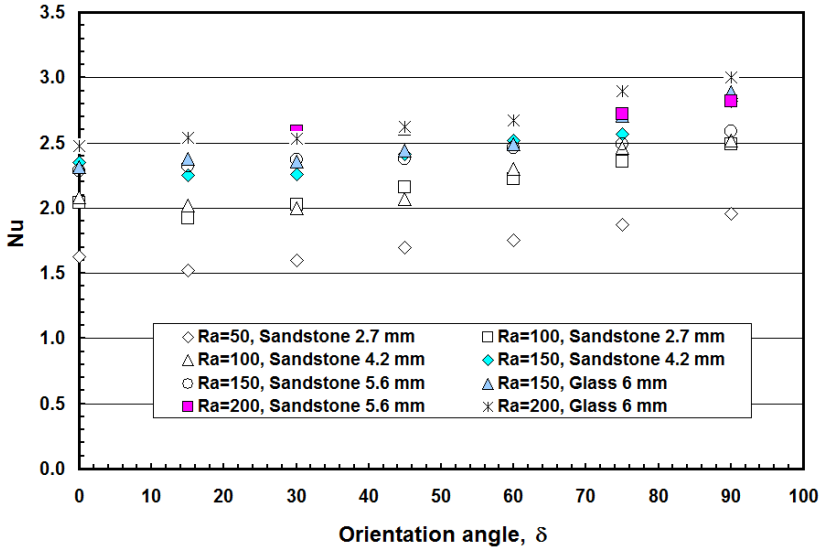

FIG. 3: Variation of the experimental results of the average Nusselt number with the orientation angle for different Rayleigh numbers (AR = 3)

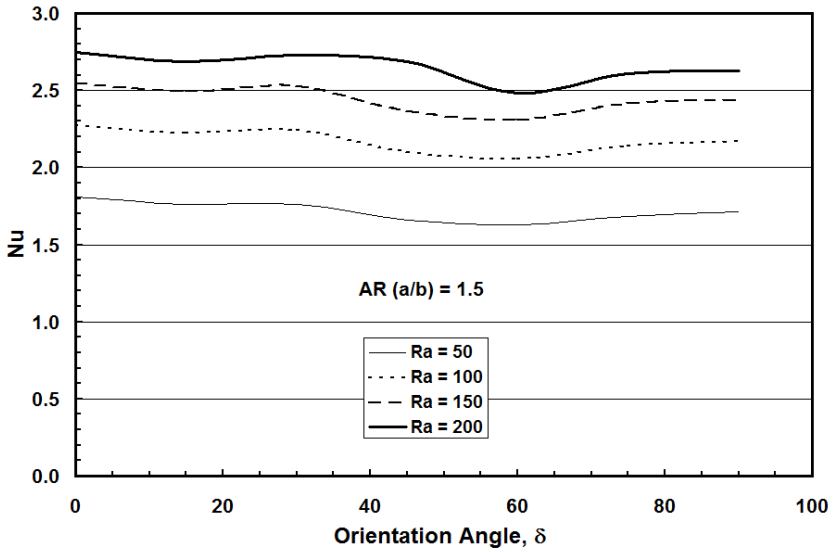

FIG. 4: Variation of the average Nusselt number with the orientation angle for different Rayleigh numbers at axis ratio of AR (a/b) = 1.5

figure that the average Nusselt number increases with the increase of Rayleigh number. Also, as the orientation angle increases, the average Nusselt number decreases and reaches its minimum value at the orientation angle of 60°, then the increase of the orientation angle increases the average Nusselt number. The same behavior is noticed in Fig. 5 for the axis ratio of the elliptic cylinder of 2.5. The minimum value of Nusselt number takes place at an orientation angle of 45°–60°, but the maximum value of Nusselt number occurs at an orientation angle of 75°. Moreover, for elliptic cylinder axis ratios of 3.0 and 5.0, Figs. 6 and 7 illustrate that the orientation angle corresponding

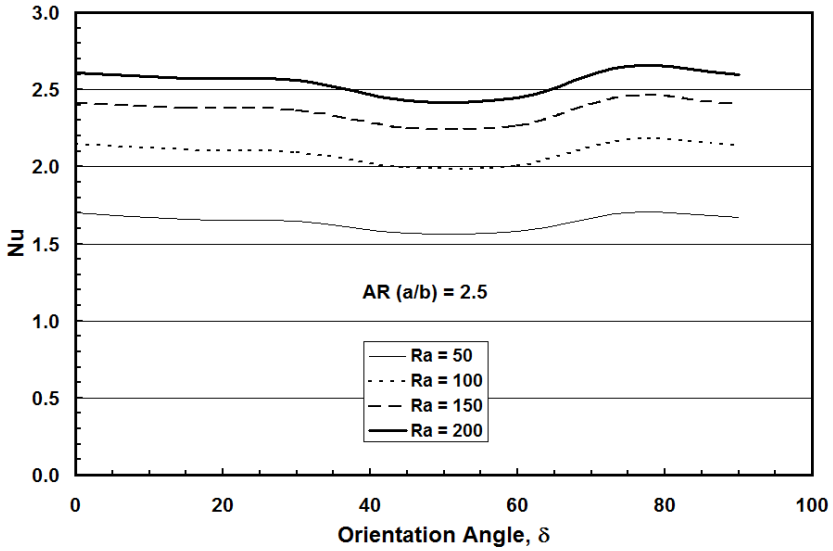

FIG. 5: Variation of the average Nusselt number with the orientation angle for different Rayleigh numbers at axis ratio of AR (a/b) = 2.5

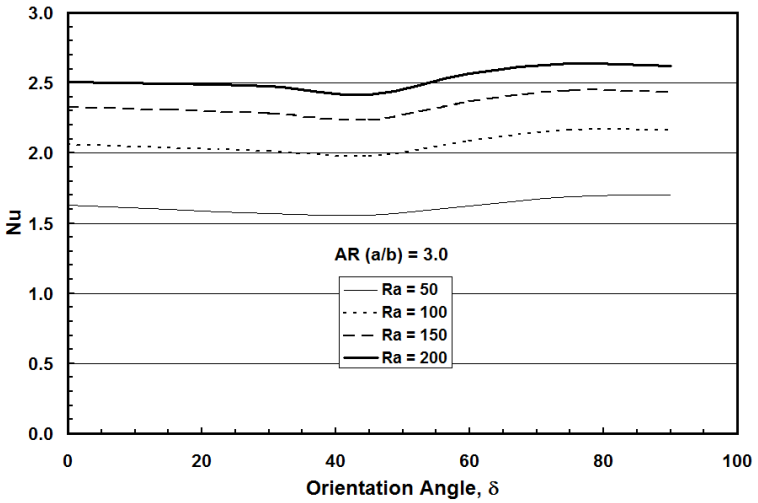

FIG. 6: Variation of the average Nusselt number with the orientation angle for different Rayleigh numbers at axis ratio of AR (a/b) = 3.0

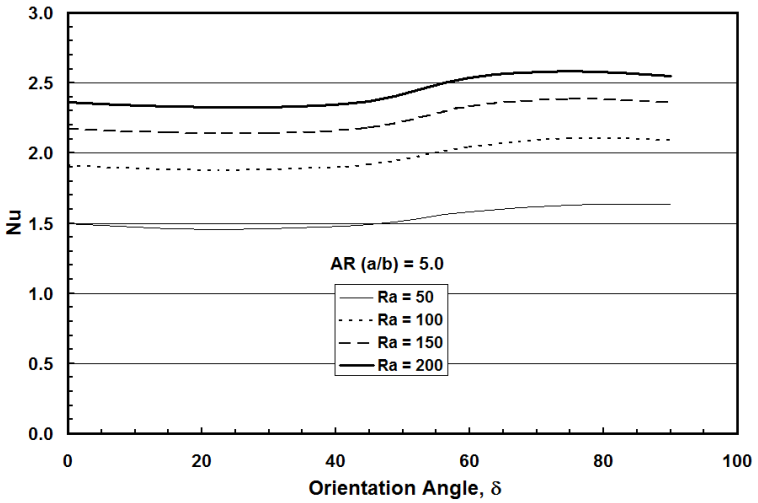

FIG. 7: Variation of the average Nusselt number with the orientation angle for different Rayleigh numbers at axis ratio of AR (a/b) = 5.0

to the minimum Nusselt number is 45° and the maximum Nusselt number takes place at an orientation angle of 75°–90°.

The variation of the average Nusselt number with Rayleigh number for different axis ratios for orientation angles of 90°, 45°, and 0°, respectively, is illustrated in Figs. 8–10. These figures show that the average Nusselt number increases with the increase of Rayleigh number and with the decrease of the axis ratio. Also, it is concluded that the influence of Rayleigh number is more significant than the axis ratio of the elliptic cylinder.

Based on the numerical predictions that are shown in Figs. 4–10, the following correlation for the average Nusselt number is obtained as a function of the different parameters:

$$\mathrm{Nu} = 0.498\mathrm{Ra}^{0.3225} AR^{-0.0777}(1+\sin\delta)^{0.0167} \quad (23)$$

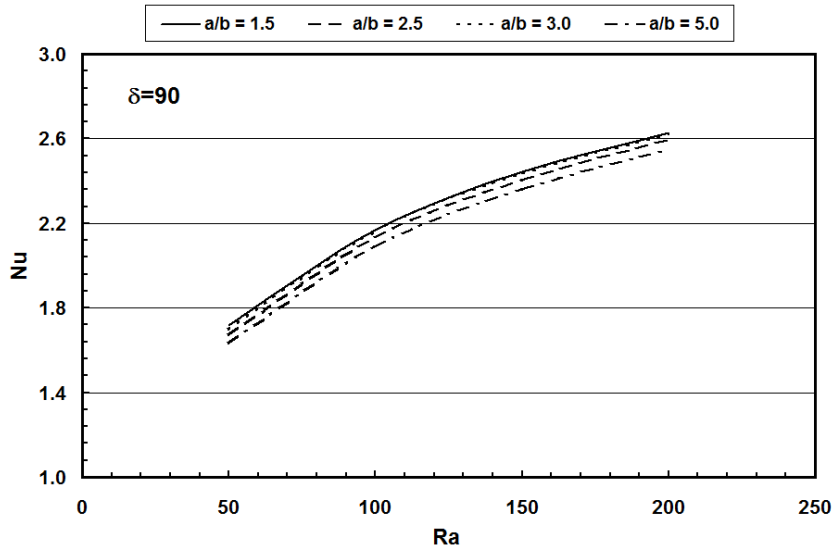

FIG. 8: Variation of the average Nusselt number with the Rayleigh number for different axis ratios at orientation angle of $\delta = 90°$

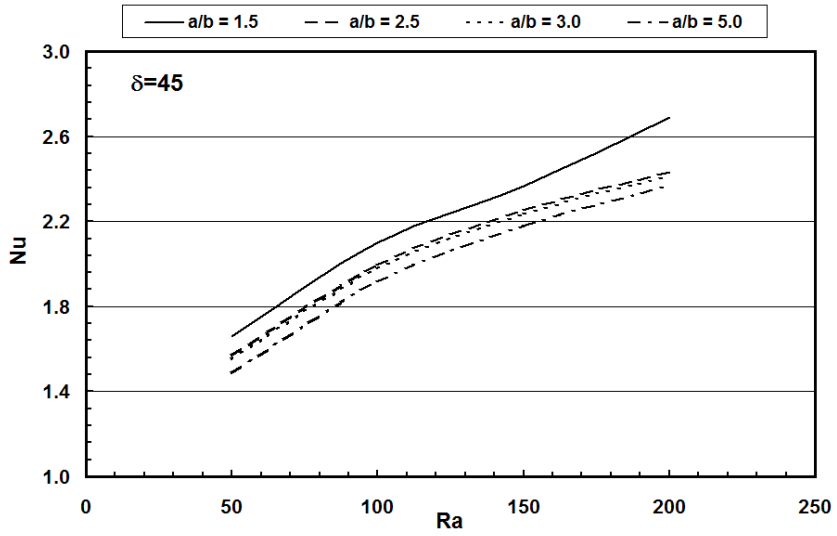

FIG. 9: Variation of the average Nusselt number with the Rayleigh number for different axis ratios at orientation angle of $\delta = 45°$

This correlation [Eq. (23)] is valid within the ranges of Rayleigh number ($50 \leq \mathrm{Ra} \leq 200$), elliptic cylinder axis ratio ($1.5 \leq AR \leq 5.0$), and orientation angle ($0° \leq \delta \leq 90°$). The maximum deviation of the numerical results from the above correlation is $\pm 7\%$.

The flow and heat transfer characteristics represented by streamfunction contours (dimensionless stream function) and isotherm contours (dimensionless temperature), respectively, are illustrated in Figs. 11(a)–11(g) for different orientation angles of the elliptic heated cylinder. This is at Rayleigh number Ra = 100 and axis ratio $AR = 3$. It is illustrated in Figs. 11(a)–11(g) that the flow in the porous annulus is considered as a two cellular flow pattern with cell centers above the elliptic cylinder. Also, the

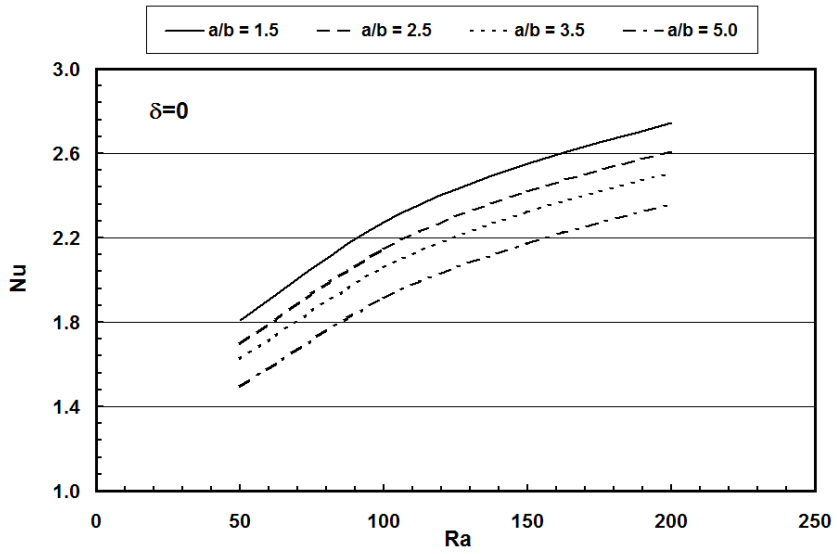

FIG. 10: Streamline (left) and isotherm (right) contours for Ra = 100 and AR = 3 for different orientation angles of the elliptic inner cylinder

change in the flow pattern with the change of the orientation angle of the elliptic cylinder is insignificant, and consequently, the corresponding change in the thermal field is insignificant (Reynolds analogy), and it is observed from the figure that the thinnest thermal boundary layer occurs at $\delta = 90°$, leading to the highest rate of heat transfer. The effect of the modified Rayleigh number on the flow and thermal fields inside the porous annulus having an elliptic cylinder axis ratio of 3 and an orientation angle $\delta = 90°$ is depicted in Fig. 12. It is noticed that as Rayleigh number increases, the values of streamfunction increase and a thinner thermal boundary layer is attained, leading to a higher rate of heat transfer and higher values of the average Nusselt number. Figure 13 shows the effect of the axis ratio $AR = a/b$ of the elliptic cylinder on the flow and heat transfer characteristics for a modified Rayleigh number of 150 and the orientation angle δ of 0°. An insignificant effect of the axis ratio on the flow and heat transfer characteristics is observed.

6.3 Comparison of Numerical Results with Experimental Data

In comparing the predictions of the present numerical model with the experimental data, Fig. 14 illustrates the variation of the average Nusselt number with the orientation angle for a modified Rayleigh number of 50 and 100, with Fig. 14(a) using sandstone grains of average diameters of 2.7 mm and 4.2 mm. To achieve higher values of Rayleigh numbers of 150 and 200, sandstone grains of average diameters of 4.2 mm and 5.6 mm as well as glass beads of 6 mm are used [Fig. 14(b)]. Fair agreement between the experimental data and the predictions is observed. This means that the present developed model is considered a good means for predicting the thermal behavior of natural convection heat transfer in an elliptic annulus containing water-saturated porous media.

7. CONCLUSIONS

Natural convection heat transfer in a horizontal elliptic annulus filled with saturated porous media was investigated experimentally and numerically. The inner horizontal elliptic tube was heated under constant heat flux conditions and was located concentrically in a larger isothermally cooled horizontal cylinder. The effects of modified Rayleigh number, elliptic cylinder orientation angle, and axis ratio of the elliptic cylinder were examined. From the foregoing results, the following conclusions can be drawn.

1. The average Nusselt number increases with the increase of the modified Rayleigh number.
2. The average Nusselt number increases with the increase of the elliptic cylinder orientation angle from

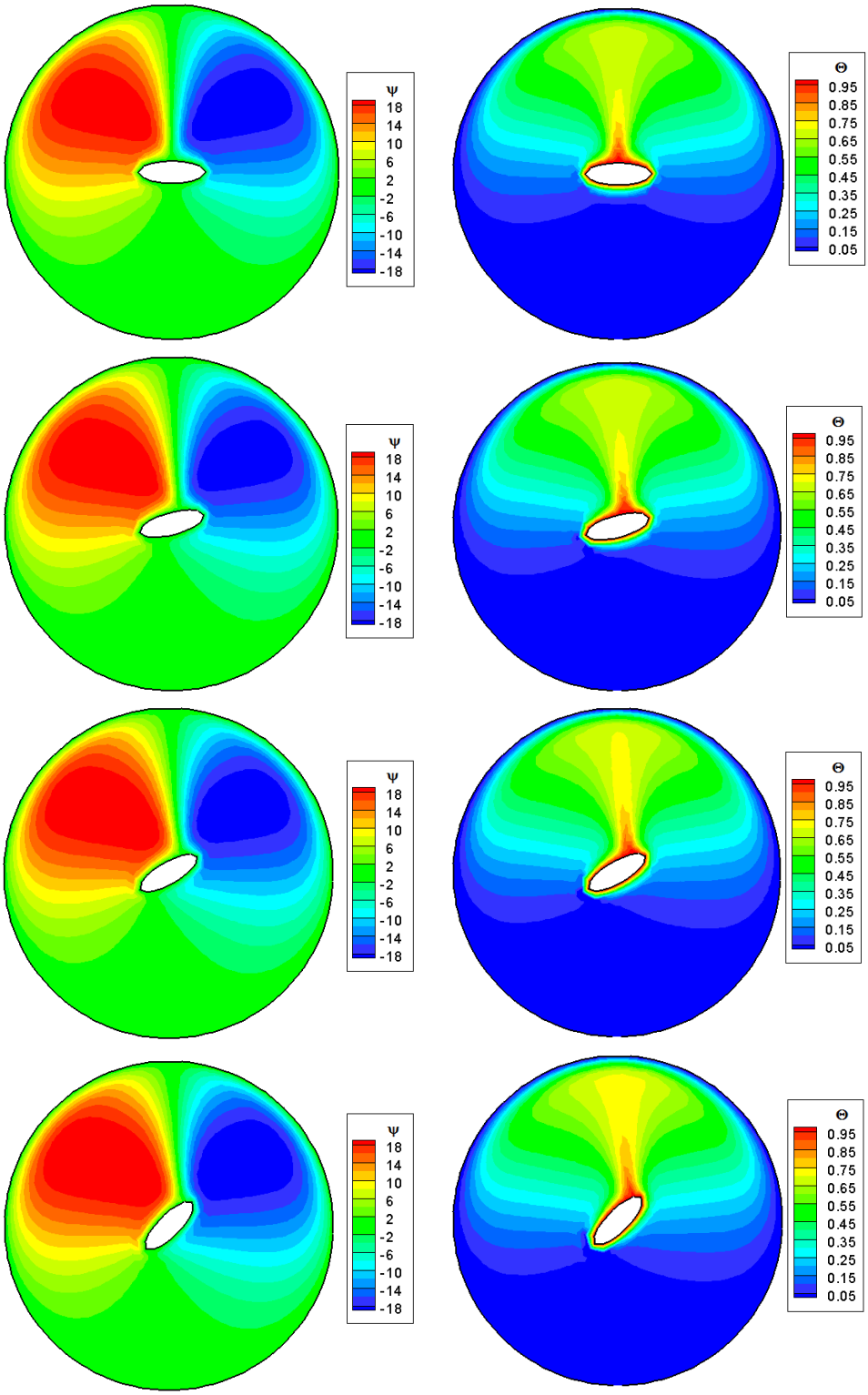

FIG. 11.

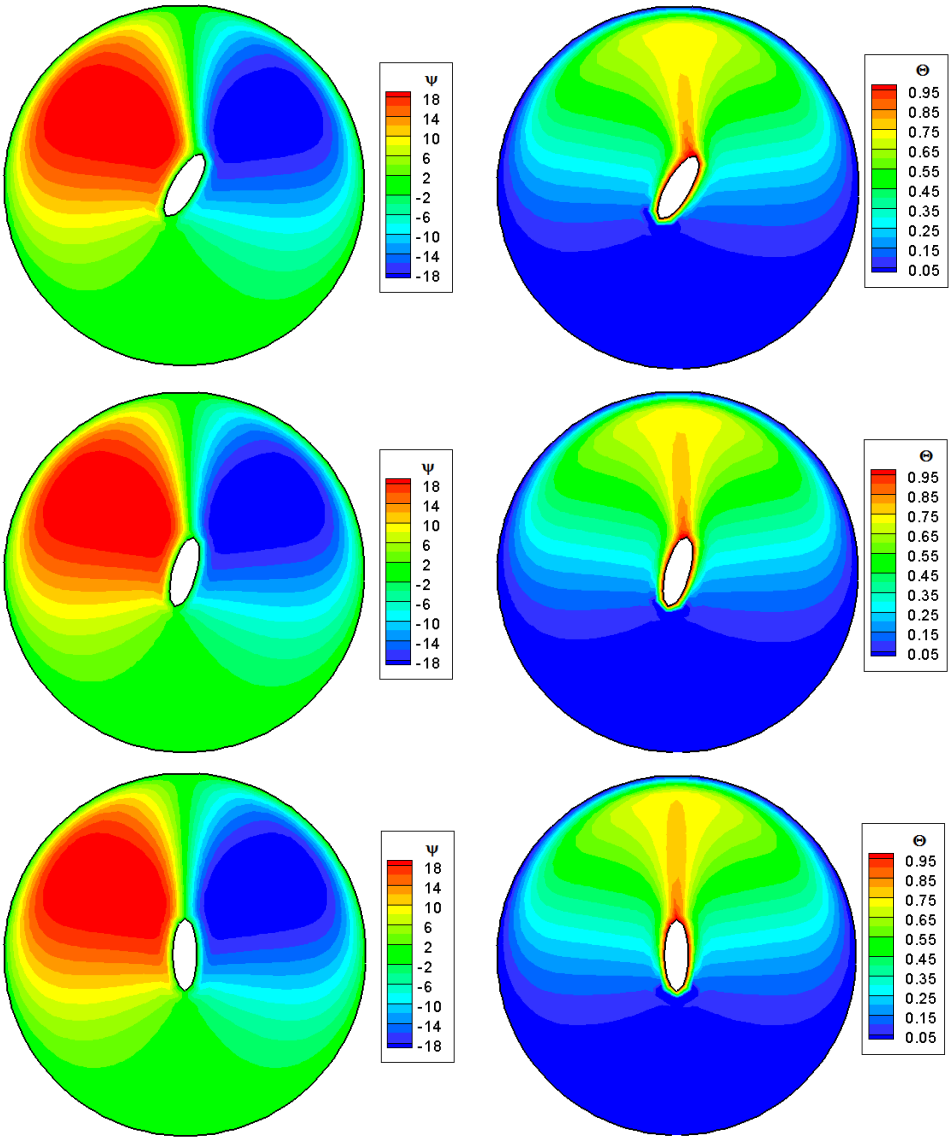

FIG. 11: Variation of the average Nusselt number with the Rayleigh number for different axis ratios at orientation angle of $\delta = 0°$

the position where its major axis is horizontal to the position of its axis is vertical.

3. There is an insignificant decrease of the average Nusselt number with the increase of the elliptic cylinder axis ratio for orientation angles other than 0°.

4. Bicellular flow pattern is dominant for all values of the modified Rayleigh numbers.

5. The effect of modified Rayleigh number, which includes the effect of fluid properties, porous medium properties, and operating conditions, on the average Nusselt number is more significant than the effect of the geometric parameters such as the elliptic cylinder orientation angle and the elliptic cylinder axis ratio.

6. The empirical correlation for the average Nusselt number is obtained as a function of Rayleigh num-

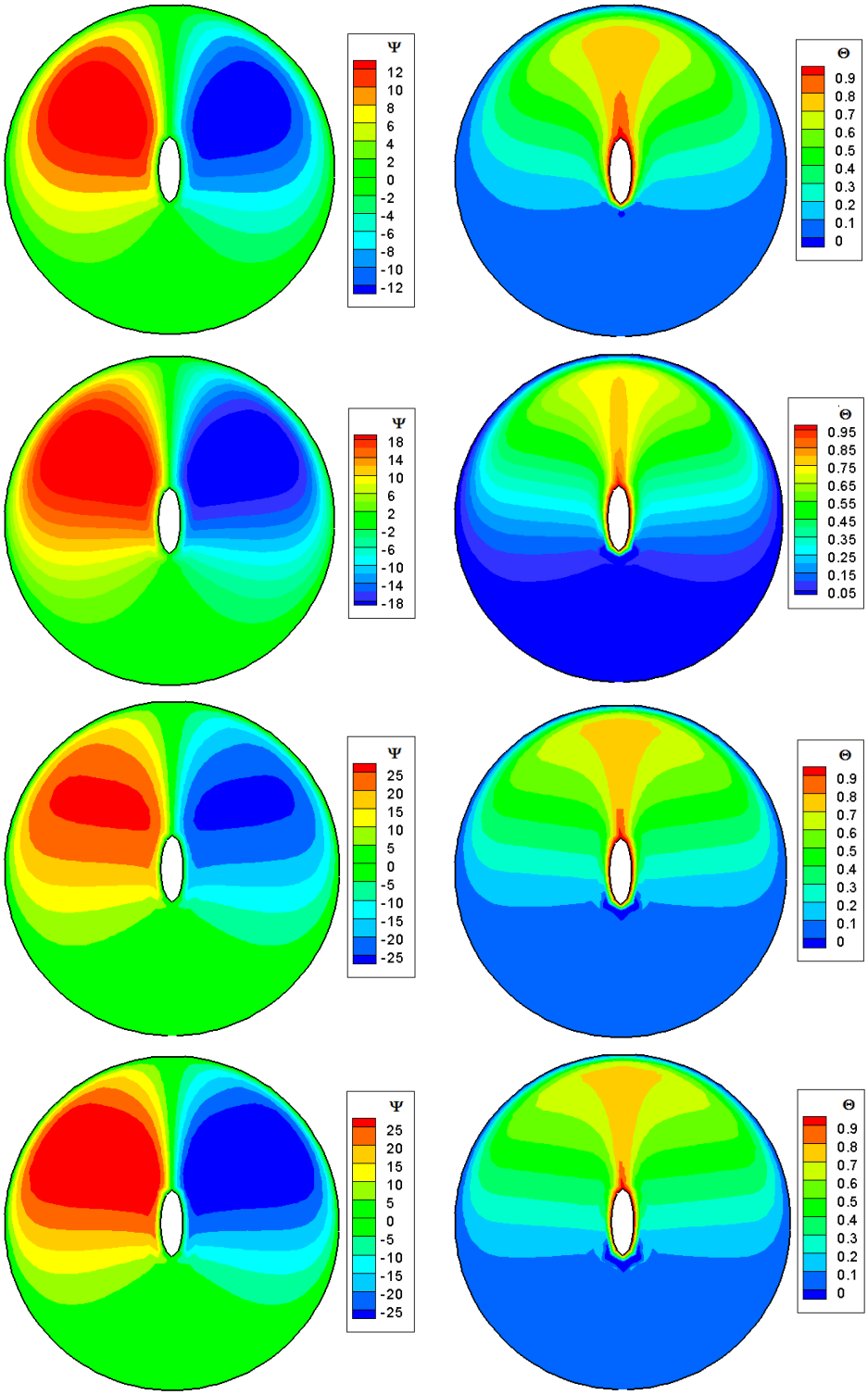

FIG. 12: Streamline (left) and isotherm (right) contours for AR = 3, $\delta = 90^\circ$ for different AR

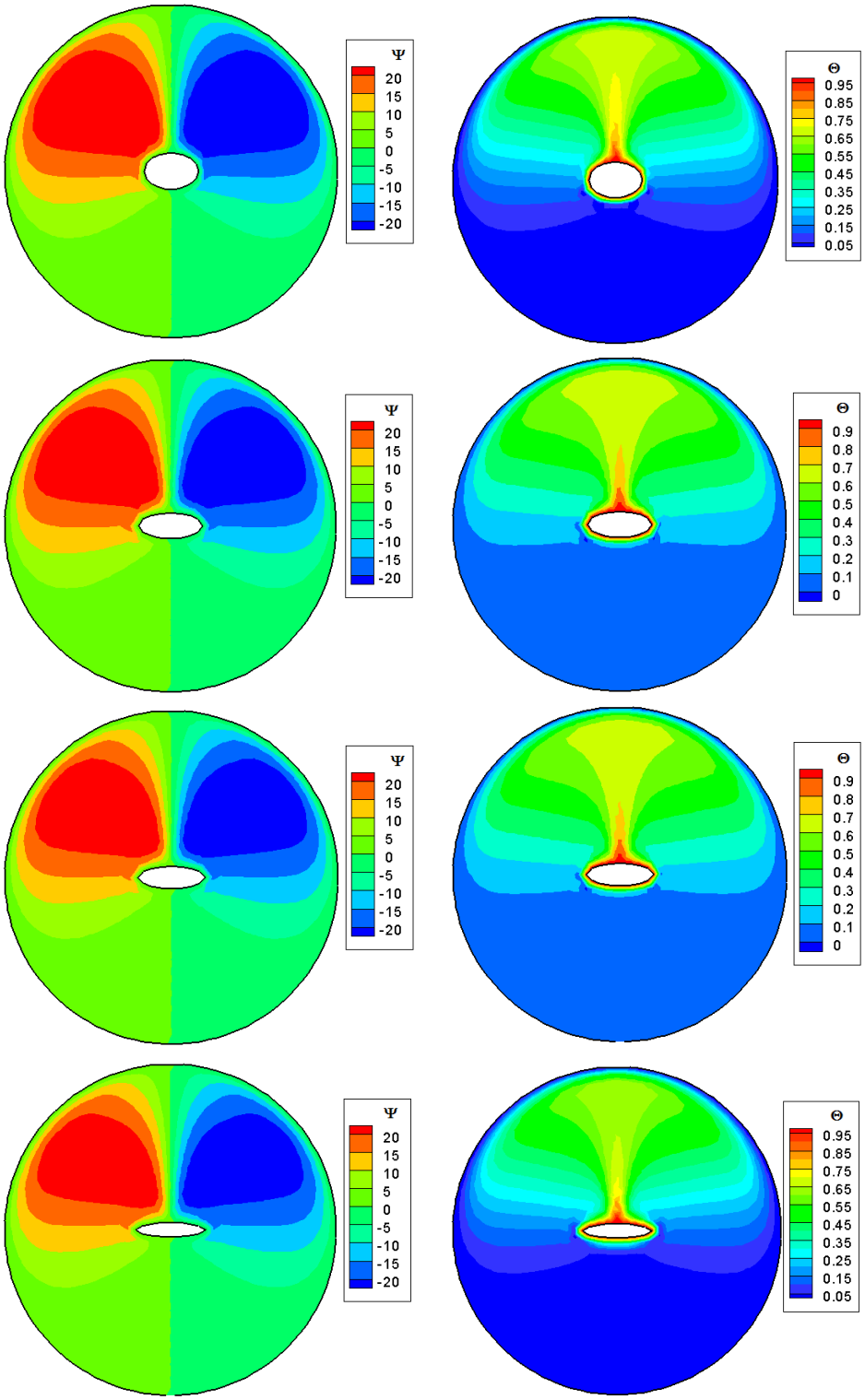

FIG. 13: Streamline (left) and isotherm (right) contours for Ra = 150, $\delta = 0°$ for different AR

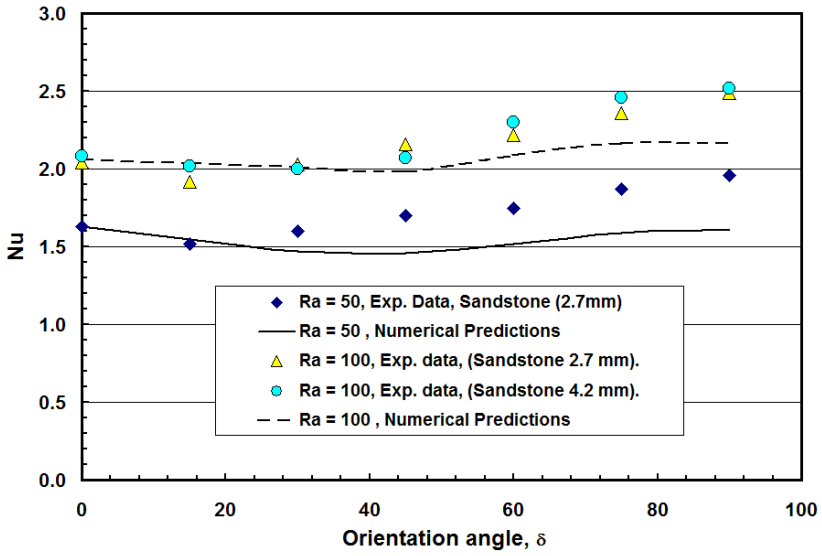

(a)

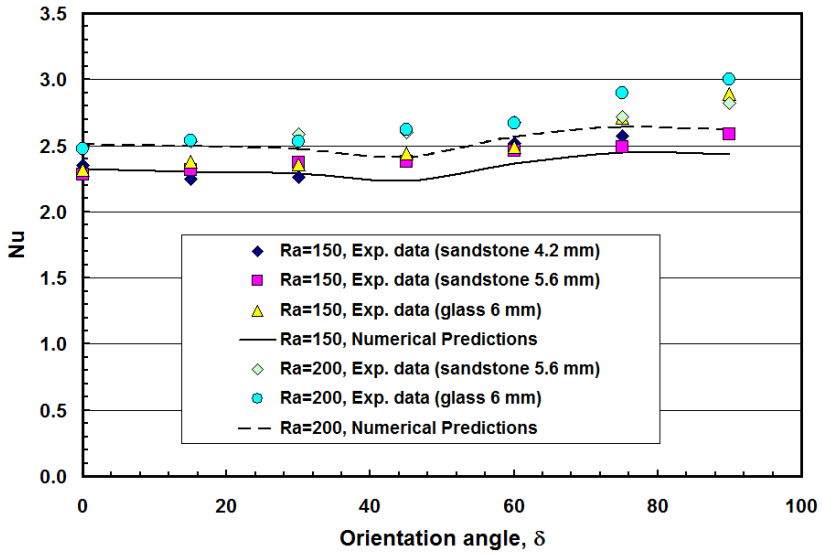

(b)

FIG. 14: Comparison between the experimental data and the numerical predictions for the average Nusselt number

ber, elliptic cylinder orientation angle, and elliptic cylinder axis ratio.

REFERENCES

Aldoss, T. K., Natural convection from a horizontal annulus filled with porous medium of variable permeability, *J. Porous Media*, vol. **12**, pp. 715–724, 2009.

Aldoss, T. K., Alkam, M., and Shatarah, M., Natural convection from a horizontal annulus partially filled with porous medium, *Int. Commun. Heat Mass Transfer*, vol. **31**, pp. 441–452, 2004.

Bau, H. H., Thermal convection in a horizontal, eccentric annulus containing a saturated porous medium—an extended perturbation expansion, *Int. J. Heat Mass Transfer*, vol. **27**, pp. 2277–2287, 1984.

Burns, J. P. and Tien, C. L., Natural convection in porous media bounded by concentric spheres and horizontal cylinders, *Int. J. Heat Mass Transfer*, vol. **22**, pp. 929–939, 1979.

Caltagirone, J. P., Thermoconvective instabilities in a porous medium bounded by two concentric horizontal cylinders, *J. Fluid Mech*., vol. **65**, pp. 337–362, 1976.

Charrier-Mojtabi, M. C., Numerical simulation of two-and three-dimensional free convection flows in a horizontal porous annulus using a pressure and temperature formulation, *Int. J. Heat Mass Transfer*, vol. **40**, pp. 1521–1533, 1997.

Cheng, C.-Y., Fully developed natural convection heat and mass transfer in a vertical annular porous medium with asymmetric wall temperatures and concentrations, *Appl. Thermal Eng*., vol. **26**, pp. 2442–2447, 2006.

Cheng, C. H. and Chao, C. C., Numerical predictions of the buoyancy-driven flow in the annulus between horizontal eccentric elliptical cylinders, *Numer. Heat Transfer A*, vol. **30**, pp. 283–303, 1996.

Chmaissem, W., Suh, S. J., and Daguenet, M., Numerical study of the Boussinesq model of natural convection in an annular space: Having a horizontal axis bounded by circular and elliptical isothermal cylinders, *Appl. Thermal Eng*., vol. **22**, pp. 1013–1025, 2002.

Djezzar, M. and Daguenet, M., Natural steady convection in space annulus between two elliptic confocal ducts: Influence of the slope angle, *ASME J*., vol. **73**, pp. 88–95, 2006.

Elshamy, M. M., Ozisik, M. N., and Coulter, J. P., Correlation for laminar natural convection between confocal horizontal elliptical cylinders, *Numer. Heat Transfer A*, vol. **18**, pp. 95–112, 1990.

Facas, G. N., Natural convection from a buried pipe with external baffles, *Numer. Heat Transfer A*, vol. **27**, pp. 595–609, 1995.

Facas, G. N. and Farouk, B., Transient and steady state natural convection in a porous medium between two concentric cylinders, *ASME J. Heat Transfer*, vol. **105**, pp. 660–663, 1983.

Jha, B. K., Free convection flow through an annular porous medium, *Int. J. Heat Mass Transfer*, vol. **48**, pp. 573–579, 2005.

Kaviany, M., Non-Darcian effects on natural convection in porous media confined between horizontal cylinders, *Int. J. Heat Mass Transfer*, vol. **29**, pp. 1513–1519, 1986.

Khanafer, K., Al-Amiri, A., and Pop, I., Numerical analysis of natural convection heat transfer in a horizontal annulus partially filled with a fluid-saturated porous substrate, *Int. J. Heat Mass Transfer*, vol. **51**, pp. 1613–1627, 2008.

Kumari, M. and Nath, G., Unsteady natural convection from a horizontal annulus filled with a porous medium, *Int. J. Heat Mass Transfer*, vol. **51**, pp. 5001–5007, 2008.

Kumari, M. and Nath, G., Unsteady natural convection flow over a heated cylinder buried in a fluid saturated porous medium, *J. Porous Media*, vol. **12**, pp. 1225–1235, 2009.

Lee, J. H. and Lee, T. S., Natural convection in the annulus between horizontal confocal elliptic cylinders, *Int. J. Heat Mass Transfer*, vol. **24**, pp. 1739–1742, 1981.

Leong, J. C. and Lai, F. C., Natural convection in a concentric annulus with a porous sleeve, *Int. J. Heat Mass Transfer*, vol. **49**, pp. 3016–3027, 2006.

Mota, J. P. B. and Saatdjian, E., Natural convection in a porous, horizontal cylindrical annulus, *J. Heat Transfer*, vol. **116**, pp. 621–626, 1994.

Mota, J. P. B. and Saatdjian, E., Natural convection in porous cylindrical annuli, *Int. J. Numer. Methods Heat Fluid Flow*, vol. **5**, pp. 3–12, 1995.

Mota, J. P. B., Esteves, I. A. A. C., Portugal, C. A. M., Esperanca, J. M. S. S., and Saatdjian, E., Natural convection heat transfer in horizontal eccentric elliptic annuli containing saturated porous media, *Int. J. Heat Mass Transfer*, vol. **43**, pp. 4367–4379, 2000.

Pepper, D. W. and Heinrich, J. C., *The Finite Element Method—Basic Concepts and Applications*, Hemisphere, Washington, 1992.

Rao, S. S., *The Finite Element Methods in Engineering*, Pergamon Press, New York, 1982.

Rao, Y. F., Fukuda, K., and Hasegawa, S., Steady and transient analyses of natural convection in a horizontal porous annulus with the Galerkin method, *J. Heat Transfer*, vol. **109**, pp. 919–927, 1987.

Rao, Y. F., Fukuda, K., and Hasegawa, S., A numerical study of three dimensional natural convection in a horizontal annulus with a Galerkin method, *Int. J. Heat Mass Transfer*, vol. **31**, pp. 695–707, 1988.

Saatdjian, E., Lam, R., and Mota, J. P. B., Natural convection heat transfer in the annular region between porous confocal ellipses, *Int. J. Numer. Methods Fluids*, vol. **31**, pp. 513–522, 1999.

Sakr, R. Y., Berbish, N. S., Abdel-Aziz, A. A., and Hanafi, A. S., Experimental and numerical investigation of natural convection heat transfer in horizontal elliptic annuli, *Int. J. Chem. Reactor Eng.*, vol. **6**, pp. 1–26, 2008.

Saravanan, S. and Kandaswany, P., Non-Darcian thermal stability of a heat generating a fluid in a porous annulus, *Int. J. Heat Mass Transfer*, vol. **46**, pp. 4863–4875, 2003.

Stewart, W. E. and Burns, A. S., Convection in a concentric annulus with heat generating porous media and a permeable inner boundary, *Int. Commun. Heat Mass Transfer*, vol. **19**, pp. 859–868, 1992.

Vasseur, P., Nguyen, T. H., Robillard, I., and Thi, V. K. T., Natural convection between horizontal concentric cylinders filled with a porous layer with internal heat generation, *Int. J. Heat Mass Transfer*, vol. **27**, pp. 337–349, 1984.